Mon. Not. R. Astron. Soc. **325,** 792–802 (2001)

Ages and metallicities of five intermediate-age star clusters projected towards the Small Magellanic Cloud

Andrés E. Piatti,[1★] João F. C. Santos, Jr,[2★] Juan J. Clariá,[1★] Eduardo Bica,[3★] Ata Sarajedini[4★] and Doug Geisler[5★]

[1]*Observatorio Astronómico, Laprida 854, 5000 Córdoba, Argentina*
[2]*Departamento de Física, ICEx, UFMG, CP 702, 30123-970 Belo Horizonte, MG, Brazil*
[3]*Universidade Federal do Rio Grande do Sul, Depto. de Astronomía, CP 15051, Porto Alegre 91500-970, Brazil*
[4]*Astronomy Department, Van Vleck Observatory, Wesleyan University, Middletown, CT 06459, USA*
[5]*Universidad de Concepción, Departamento de Física, Casilla 160-C, Concepción, Chile*

Accepted 2001 March 12. Received 2001 March 5; in original form 2000 August 30

ABSTRACT

Colour–magnitude diagrams are presented for the first time for L32, L38, K28 (L43), K44 (L68) and L116, which are clusters projected on to the outer parts of the Small Magellanic Cloud (SMC). The photometry was carried out in the Washington system C and T_1 filters, allowing the determination of ages by means of the magnitude difference between the red giant clump and the main-sequence turn-off, and metallicities from the red giant branch locus. The clusters have ages in the range 2–6 Gyr, and metallicities in the range $-1.65 <$ [Fe/H] < -1.10, increasing the sample of intermediate-age clusters in the SMC. L116, the outermost cluster projected on to the SMC, is a foreground cluster, and somewhat closer to us than the Large Magellanic Cloud. Our results, combined with those for other clusters in the literature, show epochs of sudden chemical enrichment in the age–metallicity plane, which favour a bursting star formation history as opposed to a continuous one for the SMC.

Key words: techniques: photometric – Magellanic Clouds – galaxies: star clusters.

1 INTRODUCTION

It has been well known for some time that the Magellanic Clouds contain rich star clusters of all ages (Hodge 1960, 1961). The distribution of cluster ages, however, differs strongly between the two Clouds (see e.g. Feast 1995; Olszewski, Suntzeff & Mateo 1996; Westerlund 1997). The population of recognized genuine old clusters (with ages ∼12 Gyr) in the Large Magellanic Cloud (LMC) includes possibly 15 objects, seven projected on the bar: NGC 1835, 1898, 2005, 2019, 1916, 1928 and 1939, and eight outside the bar: Reticulum, NGC 1466, 1754, 1786, 1841, 2210, Hodge 11 and NGC 2257 (Suntzeff et al. 1992; Olsen et al. 1998; Dutra et al. 1999). In contrast, although some populous metal-poor star clusters with ages between ∼5 and 9 Gyr are known in the Small Magellanic Cloud (SMC), only one object (NGC 121) is known in this galaxy with an age of ∼12 Gyr (Stryker, Da Costa & Mould 1985), comparable to the ages of the Galactic globular clusters and the oldest LMC clusters.

Regarding the intermediate-age clusters (IACs), there exists a pronounced gap in the LMC between a large number of IACs (age ∼1–3 Gyr) and the classical old globular clusters noted above (Jensen, Mould & Reid 1988; Da Costa 1991; van den Bergh 1991). The populous star cluster ESO 121–SC03 with an age of ∼9 Gyr (Mateo, Hodge & Schommer 1986) is the only IAC in the LMC within the range 3 and 12 Gyr, although recent work suggests that three other populous LMC clusters (NGC 2155, SL 663 and NGC 2121) may fall within the 'age gap' (Sarajedini 1998). As emphasized by Olszewski et al. (1996), this gap in the LMC cluster distribution also represents an 'abundance gap' in that the old clusters are all metal-poor (⟨[Fe/H]⟩ ∼ −2), while the IACs are all relatively metal-rich (Olszewski et al. 1991), approaching even the present-day abundance in the LMC (⟨[Fe/H]⟩ ∼ −0.5). In contrast, the SMC is known to have a different distribution of cluster ages from the LMC (e.g. Da Costa 1991), as it has at least six populous metal-poor star clusters with ages between ∼5 and ∼9 Gyr, namely Lindsay 113, Kron 3, NGC 339, NGC 416, NGC 361 and Lindsay 1 (Mould, Da Costa & Crawford 1984; Rich, Da Costa & Mould 1984; Olszewski, Schommer & Aaronson 1987; Mighell, Sarajedini & French 1998, hereafter MSF). Therefore, the present observational data suggest that the LMC has formed clusters in at least two different bursts, whereas the SMC has formed clusters more uniformly over the past 12 Gyr (although see Rich et al. 2000 for evidence favouring bursts in SMC cluster formation as well). The relationship between age and metallicity among the star

★E-mail: andres@iafe.uba.ar (AEP); jsantos@fisica.ufmg.br (JFCS); claria@mail.oac.uncor.edu (JJC); bica@if.ufrgs.br (EB); ata@urania.astro.wesleyan.edu (AS); doug@kukita.cfm.udec.cl

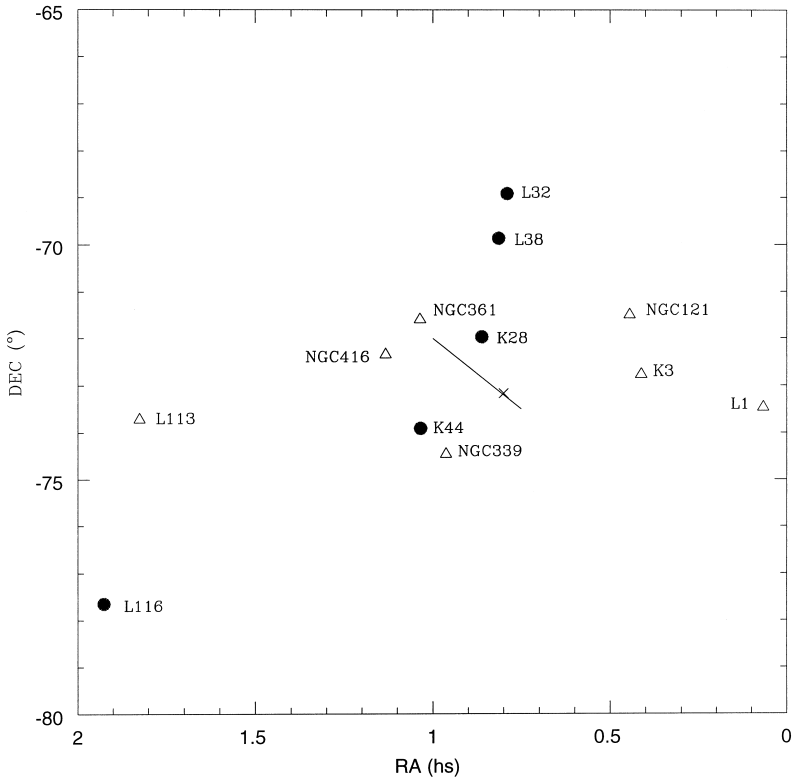

Figure 1. The position of the five studied cluster fields (filled circles) with relation to the SMC bar (straight line) and optical centre (cross). Clusters with ages given by Mighell et al. (1998) are also shown as open triangles.

clusters in both galaxies provides fundamental insight into their star formation/chemical enrichment history. Recent summaries of the LMC and SMC age–metallicity relations may be found in Olszewski et al. (1996), Geisler et al. (1997), Bica et al. (1998), MSF, Da Costa & Hatzidimitriou (1998) and Da Costa (1999). However, although ages and abundances for well-studied clusters in the SMC are well established, a larger sample of SMC clusters with age/metallicity data is needed to fill out the observed cluster age–metallicity relationship. Unlike the LMC, the SMC does not have a cluster 'age gap' that would prevent one from using its star clusters to learn about details of the age–metallicity relationship of the galaxy. Existing SMC cluster age–metallicity relationships vary widely: e.g. that of Da Costa & Hatzidimitriou (1998) shows continuous enrichment from the oldest to the youngest clusters and suggests the data are well fitted by a closed box chemical evolution model, with a few anomalously metal-poor clusters at intermediate ages, while that of Olszewski et al. (1996) shows essentially no chemical enrichment from ∼10 Gyr ago until only ∼1–2 Gyr ago, when the metallicity increased very rapidly. Clearly, more clusters are needed to define this relationship more accurately.

The goal of the present paper is twofold: (1) to derive age and metallicity for a sample of five intermediate-age cluster candidates projected towards the SMC using new CCD Washington C, T_1 photometry, and (2) to compare the cluster properties with those of their surrounding fields. The present data are particularly useful to improve our understanding of the age and metal-abundance distributions and stellar content of SMC clusters.

The selected IAC candidates are: Lindsay 32 (L32) or ESO 51-SC2, Lindsay 38 (L38) or ESO 51-SC3, Kron 28 (K28) also known as Lindsay 43 (L43), Kron 44 (K44) also known as Lindsay 68 (L68) and Lindsay 116 (L116) or ESO 13-SC25, where cluster designations are from Kron (1956), Lindsay (1958) and Lauberts (1982). All these clusters were considered IAC candidates based on their smooth structure and brightness distribution of the stars, as seen on ESO/SERC Schmidt plates. Fig. 1 shows their positions in relation to the SMC bar. K28 and K44 are near the edge of the SMC main body. If the position (J2000): $00^h49^m27^s$, $-73°09'30''$ is assumed to be the centre of the SMC bar, K28 is located at $\approx 1.^\circ 1$ to the north, and K44 the same amount to the south-east. L32 and L38 at $\approx 4.^\circ 2$ and $3.^\circ 3$, respectively north of the bar, are among the outermost SMC clusters. Finally, L116 at $6.^\circ 1$ south-east of the bar centre is the outermost projected cluster, except for objects located in the Bridge (Lindsay 1958, Bica & Schmitt 1995). No colour–magnitude diagram (CMD) has been obtained so far for any of these SMC objects.

This paper is structured as follows: Section 2 presents the observations, while Section 3 describes the cluster and field CMDs. Section 4 focuses on ages and metallicities. Section 5 discusses the age–metallicity relationship in the SMC and its implication for star cluster formation. Finally, Section 6 deals with the conclusions of this work.

2 OBSERVATIONS

The five SMC clusters and surrounding fields were observed during four photometric nights with the Cerro Tololo Inter-American Observatory (CTIO) 0.9-m telescope in 1998 November with the Tektronix 2K #3 CCD, using quad-amp readout. The scale on the chip is 0.4 arcsec per pixel, yielding an area covered by a frame of 13.5×13.5 arcmin^2. The integrated IRAF[1]-Arcon 3.3 interface for

[1]IRAF is distributed by the National Optical Astronomy Observatories, which is operated by the Association of Universities for Research in Astronomy, Inc., under contract with the National Science Foundation.

direct imaging was employed as the data acquisition system. A mean gain of 1.5 e^- ADU^{-1} and a mean readout noise of 4.2 e^- resulted for the chosen settings. We obtained data with the Washington (Canterna 1976) C and Kron–Cousins R filters. The latter has been shown to be an efficient substitute for the standard Washington T_1 filter (Geisler 1996). Exposures of 40 min in C and 15 min in R_{KC} were taken for the SMC fields. Their airmasses were always less than 1.5 and the seeing was typically 1 arcsec. The observations were supplemented with nightly exposures of bias, dome- and twilight sky-flats to calibrate the CCD instrumental signature. Several LMC fields were also observed in the same run using the same technique and they were presented in Piatti et al. (1999), where a detailed description of the data collection and reduction procedures is given. In summary, the DAOPHOT II/ALLSTAR stand-alone package (Stetson 1994) was used to obtain the photometry for which the typical magnitude and colour errors provided by DAOPHOT II are shown in Fig. 2. It shows a typical trend of T_1 and $(C - T_1)$ photometric errors with T_1, for the cluster K44 and for its rich associated field. For the 49 857 stars measured in all clusters and fields, the mean magnitude and colour errors for stars brighter than $T_1 = 19$ were $\sigma(T_1) = 0.016$ and $\sigma(C - T_1) = 0.029$; for stars brighter than $T_1 = 21$, $\sigma(T_1) = 0.042$ and $\sigma(C - T_1) = 0.063$. Although our photometry reaches only slightly deeper than the turn-off magnitudes, its quality allowed us to detect and measure the turn-off for all of them, which was used in our age estimates. Indeed, by using the relation between the turn-off R magnitude and age according to theoretical isochrones by Bertelli et al. (1994) and by comparing it with our data, we concluded that we are able to define turn-offs for stellar populations as old as 6.3 ± 1.1 Gyr ($R \approx 22$) with an error of 0.2 in R. Slightly fainter turn-offs can be reached at expenses of larger errors. On each photometric night, a large number (typically 19–32) of standard stars from the list of Geisler (1996) were also observed. Care was taken to cover a wide colour and airmass range for these standards in order to calibrate the programme stars properly. Table 1 presents the logbook of observations of the SMC

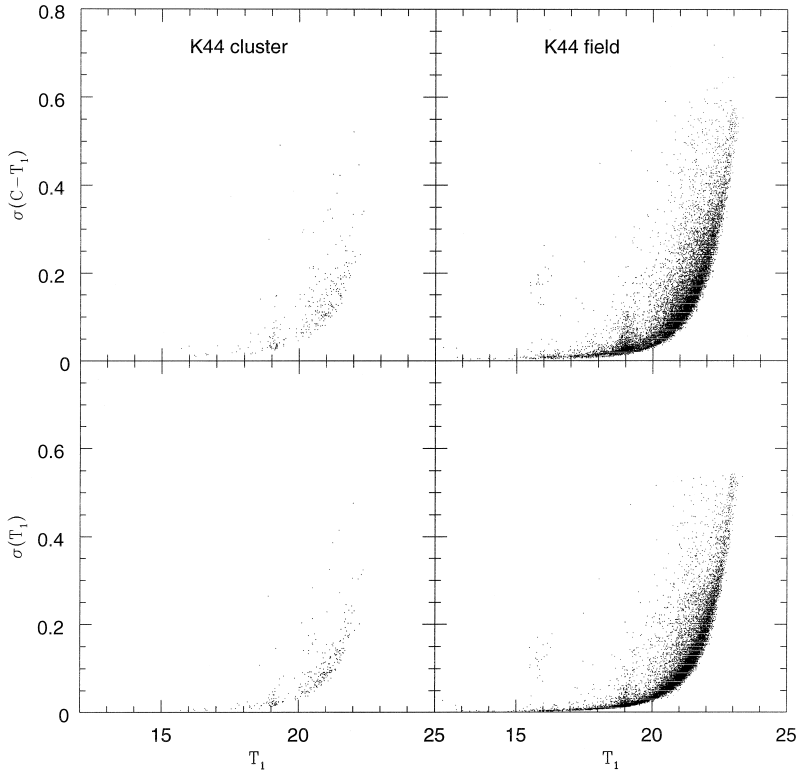

Figure 2. Magnitude and colour photometric errors provided by DAOPHOT II as a function of T_1 for a rich field (K44) and its associated cluster. They are typical in our sample.

Table 1. Observation log.

Cluster fields	α_{2000} (h m s)	δ_{2000} (° ′ ″)	ℓ (°)	b (°)	date	airmass	seeing (arcsec)
L32=ESO 51-SC2	00 47 24	−68 55 10	303.48	−48.20	20/11/1998	1.28	1.0
L38=ESO 13-SC3	00 48 50	−69 52 11	303.26	−47.26	22/11/1998	1.32	1.1
K28=L43	00 51 42	−71 59 52	302.90	−45.13	19/11/1998	1.34	1.0
K44=L68	01 02 04	−73 55 31	301.92	−43.18	18/11/1998	1.40	1.0
L116=ESO 13-SC25	01 55 33	−77 39 16	298.58	−38.93	18/11/1998	1.49	1.0

Cluster identifications are from Lindsay (1958, L) and Kron (1956, K).
The exposure times were 15 min for R and 40 min for C.

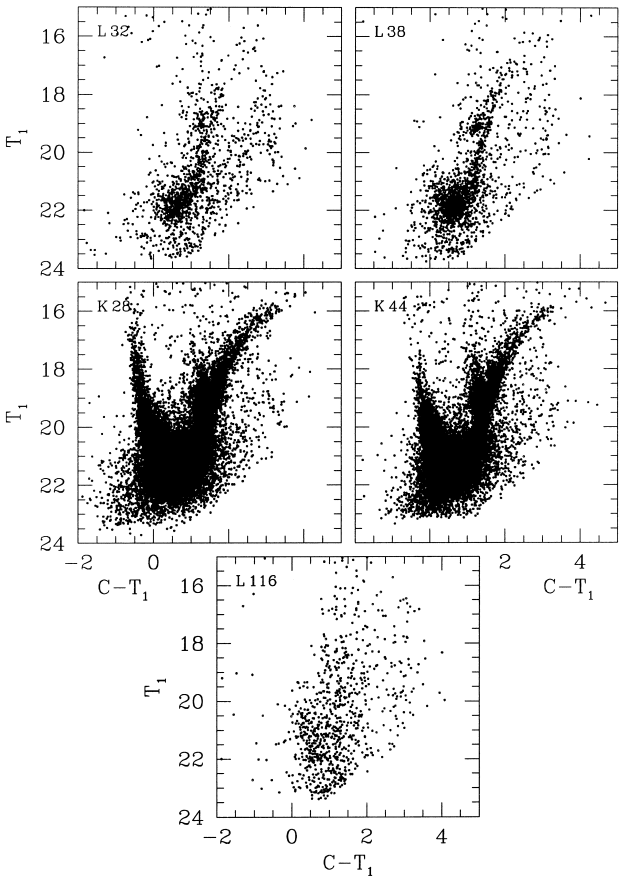

Figure 3. Washington T_1 versus $C - T_1$ CMDs for all the measured stars in the cluster fields.

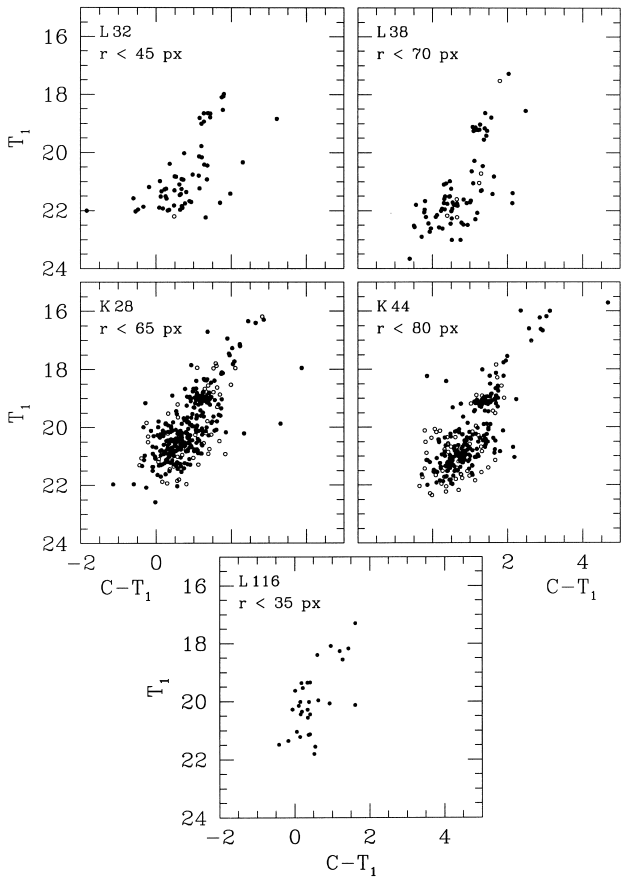

Figure 4. Washington T_1 versus $C - T_1$ CMDs of star clusters. Filled circles represent probable cluster members and open circles removed objects (see Section 3 for details). Extraction radius in pixels is given in each panel.

cluster fields while Fig. 3 shows the CMDs for the entire observed field around each cluster. The data are available from the first author upon request.

3 ANALYSIS OF THE COLOUR–MAGNITUDE DIAGRAMS

The relatively large size of the field of view allowed us not only to properly sample the entire extent of each cluster but also to sample a significant area of their surrounding field. To build cluster CMDs, we estimated the cluster radii by eye, selecting a limiting radius within which most of the cluster's light seemed to fall. The estimated radii range between 35 (14 arcsec) and 80 (32 arcsec) pixels, with a typical radius of 60 (24 arcsec) pixels. Fig. 4 shows the resulting cluster CMDs using all the observed star within the adopted radii. All the clusters exhibit clear red giant clumps (RGCs) near $T_1 \sim 19$ and Main Sequence (MS) turn-offs which lie roughly 0.50–0.75 mag above the limit of our photometry, except for L116, the features of which are more difficult to identify.

Before estimating cluster ages and metallicities, we cleaned the cluster CMDs of stars that can potentially belong to the foreground/background fields. We used four circular extractions placed well beyond the clusters and distributed throughout the observed fields. The four field regions have radii that equal half of the radius corresponding to the cluster in that field, so that the total field comparison area is equal to that of the cluster area. We then built field CMDs and counted how many stars lie in different magnitude–colour boxes with sizes $[\Delta T_1,\ \Delta(C - T_1] = (0.5, 0.5)$ mag. We then subtracted from each cluster CMD the number of stars counted in the corresponding field CMD in each (T_1, $C - T1$) bin, subtracting the star closest to that of each field star. In Fig. 4 we represent remaining cluster stars with filled circles and subtracted stars with open circles. In the subsequent analysis we used the former as defining the fiducial cluster sequences. Although the cleaned cluster CMDs may still contain some field interlopers, the CMDs of K28 and K44 now appear to be better defined.

On the other hand, more cluster stars should also be at distances larger than the adopted radii, at least as far as cluster stellar density profiles extend (see discussion below). Fig. 5 shows the resulting cluster CMDs for circular extractions (open clusters) with radii three times larger than the adopted cluster radii, as well as cluster stars which define fiducial sequences (filled circles) superimposed (see Fig. 4). As can be seen, the RGC of L32 includes some additional stars, the red giant branch of L38 is much better defined and the CMD of L116 has more RGC stars and a more populated MS down to fainter magnitudes. The CMDs of K28 and K44, although containing more cluster stars, also show much greater contamination from SMC field stars and are presented for completeness purposes only. To estimate cluster ages and metallicities we used these larger circular extraction CMDs weighted by the fiducial cluster stars.

Surrounding cluster field CMDs also need to be cleaned from contamination by cluster and foreground/background stars in order to determine their fundamental parameters and to compare properties of clusters and associated SMC fields. Cluster extents

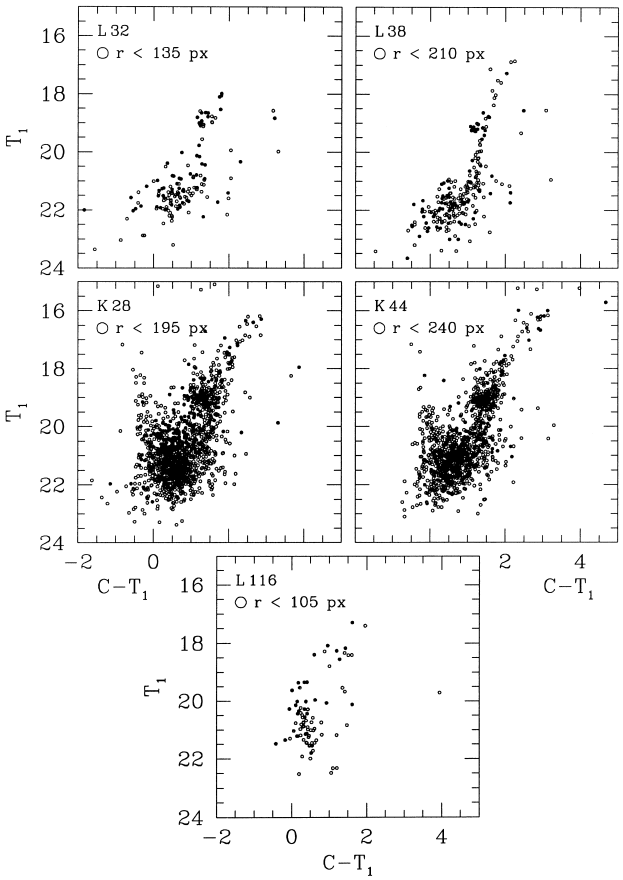

Figure 5. Washington T_1 versus $C - T_1$ CMDs of star clusters. Filled circles are the same as in Fig. 4 and open circles represent stars from the larger circular extraction (see Section 3 for details). The radius in pixels of the larger circular extraction is given in each panel.

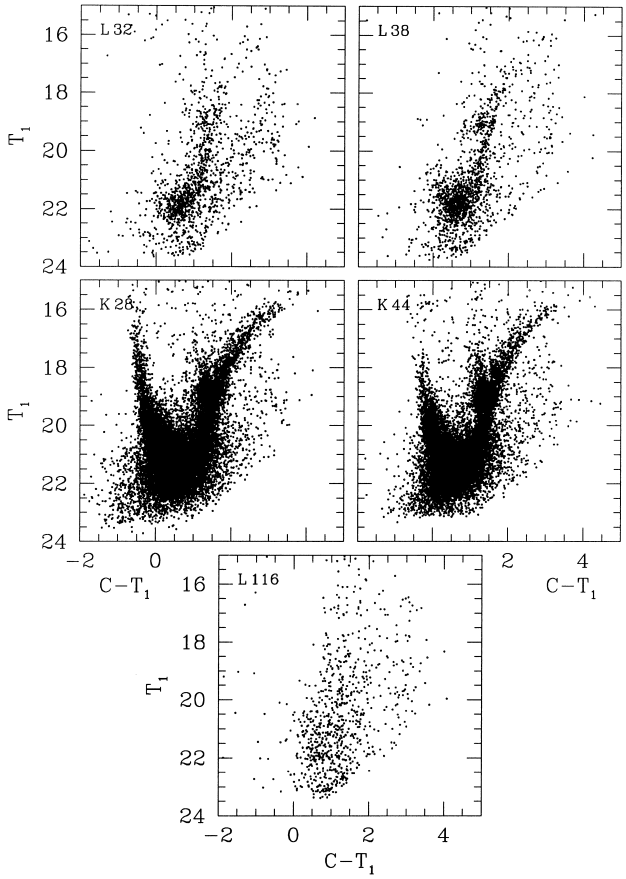

Figure 6. Washington T_1 versus $C - T_1$ CMDs of the surrounding fields, excluding areas of radius three times that of the cluster.

were then delimited by adopting as field stars objects beyond three cluster radii. This criterion statistically constrains cluster star contamination in the field CMDs at a confidence level higher than 95 per cent. Fig. 6 shows the resulting field CMDs plotted using all the star located between 3 × (cluster radius) and CCD boundaries. The CMDs of the two inner SMC clusters of the sample (K28 and K44) clearly reveal the main SMC field features, characterized by the mixture of young and old stellar populations. The most obvious features are the long MS which extends approximately 7 mag in T_1, the populous and broad subgiant branch, indicator of the evolution of stars with ages (masses) within a non-negligible range, the RGC and the red giant branch (RGB). The RGC is somewhat elongated in T_1 and appears to be populated at brighter magnitudes by the so-called 'vertical red clump' structure (see e.g. Zaritsky & Lin 1997; Gallart 1998; Ibata, Lewis & Beaulieu 1998). However, no evidence for the vertical structure stars seen in some LMC fields (Piatti et al. 1999) exists.

Surrounding field CMDs are more affected by the presence of stars that belong either to the SMC or to the foreground Galactic field than by contamination from cluster stars. As these Galactic field stars are distributed over the entire field of view, we applied the statistical procedure described by MSF in order to remove them from the surrounding field CMDs. We assume that the Galactic field is well represented by the surrounding field CMD of L116, because it has no evidence of clump or horizontal branch (HB) or turn-off of any kind, so that no SMC field stellar population is detected in this frame. The method is suitably designed to clean CMDs in which the intrinsic features are well defined by many stars, as is the case for K28 and K44. Note that the cleaning method was only applied to L32 and L38 fields for completeness purposes, because RGCs and MS turn-offs are clearly visible in the observed CMDs. In Fig. 7 we present probable SMC stars. The main features of the surrounding fields CMDs of K28 and K44 are now better defined, especially the most evolved ones, as expected.

4 AGES AND METALLICITIES

4.1 Star clusters

The magnitude difference between the clump/HB and the turn-off has proved to be a useful tool for estimating ages of IACs and old clusters as well (see Phelps, Janes & Montgomery 1994 and references therein). Geisler et al. (1997) calibrated this difference for the T_1 magnitude of the Washington system and applied it to a sample of LMC IACs. Following the same method, we used their calibration for estimating ages of our cluster sample. δT_1 magnitude differences were measured on CMDs of Fig. 5, assigning more weight to fiducial stars (filled circles). The cluster RGCs have an average magnitude of $T_{1_{\rm clump}} \approx 19.0 \pm 0.1$ mag, except for L116 whose RGC lies at $T_{1_{\rm clump}} = 18.2 \pm 0.1$ mag. This suggests that L116 is located not only several degrees from the SMC bar but also in front of it (see Section 5). Cluster turn-offs were more difficult to determine, mainly because of intrinsic dispersion and photometric errors at these faint magnitudes. This was especially true for L116, which is particularly sparse. Its turn-off appears to lie either at $T_1 \sim 19.5$ or 20.2. Our preferred value is

the latter, leading to an age of 2.8 Gyr; the former value yields 1.6 Gyr. Clearly, the age for this cluster is particularly uncertain. Photometric errors at the turn-off level were always $(\sigma)T_1 \leq 0.15$–0.20 mag. The mean δT_1 values and their errors were estimated from independent measurements of turn-off points and RGCs by three authors using lower and upper limits in order to take into account the intrinsic dispersion. The difference between maximum and minimum δT_1 values resulted in $\Delta(\delta T_1) \approx 0.2$–$0.4$ mag. Table 2 lists the resulting cluster ages computed with equation (4) of Geisler et al. (1997). We would like to ensure that our age scale is the same as that of MSF, in which L1 is 9 ± 1 Gyr old. We measured $\delta V = 3.0 \pm 0.1$ for L1, which transforms into $\delta T_1 = 3.1 \pm 0.1$ using equation (3) of Geisler et al. (1997), resulting in an age of 9.5 ± 1.0 Gyr. This value is in good agreement with that derived by Olzsewski et al. (1996) and Rich et al. (2000) and adopted by MSF. We did not apply any offset to our age scale because it is within the errors and we want to maintain consistency with the previous age scale of Bica et al. (1998).

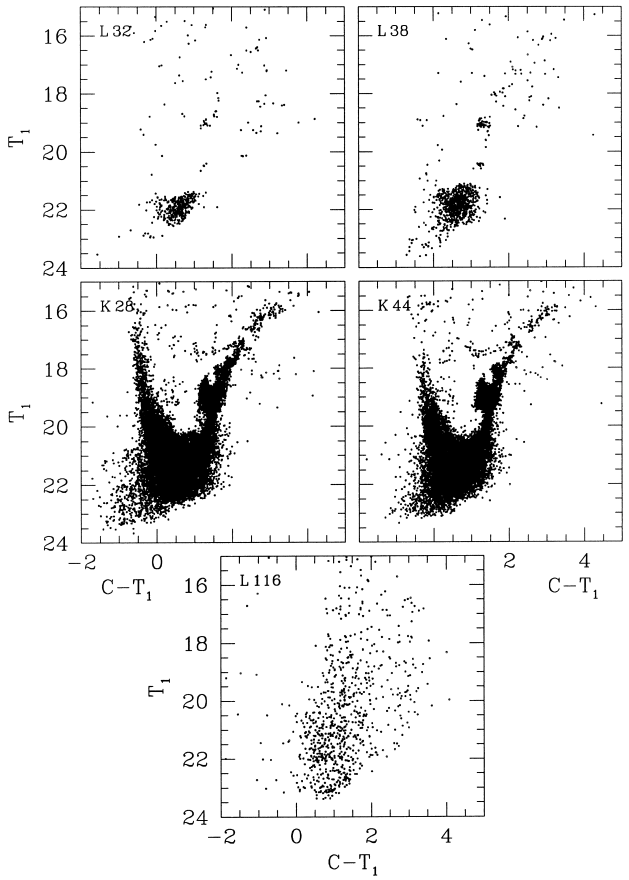

Figure 7. Washington T_1 versus $C - T_1$ CMDs of the surrounding fields as in Fig. 6, statistically cleaned from foreground star contamination (see Section 3 for details).

Table 2. Ages of SMC clusters and surrounding fields.

Name	δT_1 (mag)	$\text{Age}_{\text{cluster}}$ (Gyr)	δT_1 (mag)	$\text{Age}_{\text{field}}$ (Gyr)
L32	2.5 ± 0.1	4.8 ± 0.5	2.8 ± 0.2	6.7 ± 0.8
L38	2.7 ± 0.1	6.0 ± 0.6	2.6 ± 0.1	5.4 ± 0.2
K28	1.7 ± 0.3	2.1 ± 0.5	2.3 ± 0.1	3.7 ± 0.4
K44	2.1 ± 0.2	3.1 ± 0.8	1.8 ± 0.1	2.2 ± 0.2
L116	2.0 ± 0.4::	2.8 ± 1.0::	–	–

As noted above, no previous CMDs exist for any of these clusters. Some age information does exist for K44, however. Elson & Fall (1985) found K44 to be among the oldest SMC clusters, based on their *s* value of 47 derived from the integrated $(U - B) : (B - V)$ diagram. This *s* value is the same one they find for NGC 121, generally accepted to be the oldest SMC cluster, with an age of ~12 Gyr (e.g. Rich et al. 2000). A search for RR Lyraes in K44 by Walker (1998) did not turn up any candidates, indicating an age <10 Gyr. We find this cluster to be only a few Gyr old. Geisler et al. (1997) discussed the problems inherent in deriving reliable ages from integrated *UBV* photometry of faint clusters in crowded fields and it appears that the Elson & Fall estimate for K44 may suffer from this same effect.

Cluster metallicities were derived by interpolating by eye in the standard giant branches of the Washington system recently defined by Geisler & Sarajedini (1999). They demonstrated that this technique is three times more sensitive to metallicity than the corresponding $V - I$ technique of Da Costa & Armandroff (1990). To trace the standard giant branches, they used the mean loci of giant and subgiant branches of Galactic globular and several old open clusters with known metallicities as fiducial clusters. We then entered in their M_{T_1} versus $(C - T_1)_o$ diagram the T_1 magnitudes and $C - T_1$ colours for our cluster stars, previously corrected for foreground reddening and distance, and estimated the mean cluster metallicities. Note that Geisler & Sarajedini (1999) derived their metallicity calibration for three metallicity scales – here we use the Zinn (1985) scale. Reddening and distance corrections were performed using the expressions $E(C - T_1) = 1.97E(B - V)$ and $M_{T_1} = T_1 + 0.58E(B - V) - (m - M)_V$ (Geisler & Sarajedini 1999). For the SMC clusters, we assumed an apparent distance modulus $(m - M)_V = 19.0$, except for L116, taking into account results recently obtained by Cioni et al. (2000) using data extracted from the DENIS catalogue towards the Magellanic Clouds. We used a foreground reddening $E(B - V)$ depending on the Galactic coordinates (Table 1) and the values from the maps by Burstein &

Table 3. Reddenings and metallicities of SMC clusters and surrounding fields.

Name	$E(B - V)_{\text{BH}}$	$E(B - V)_{\text{SFD}}$	$[\text{Fe/H}]^*_{\text{cluster}}$	$[\text{Fe/H}]^*_{\text{field}}$
L32	0.00	0.02	-1.2 ± 0.2	-1.5 ± 0.2:
L38	0.02	0.02	-1.65 ± 0.2	-1.7 ± 0.2
K28	0.06	0.16	$-1.2(-1.45) \pm 0.2$	$-1.2(-1.45) \pm 0.2$
K44	0.03	0.05	-1.1 ± 0.2	-0.9 ± 0.2
L116	0.06	0.05	-1.1 ± 0.2::	—

* Metallicities were corrected by +0.4 and +0.2 for ages between 1–3 and 3–5 Gyr. (See Section 4 for details.)

Heiles (1982, hereafter BH) and Schlegel, Finkbeiner & Davis (1998, hereafter SFD). SFD produced a full-sky map of the Galactic dust based upon its far-infrared emission (100 μm), which allowed us to check the BH values. SFD have not removed the SMC so that we could take into account not only possible Galactic dust variations but also the internal SMC reddening, especially in the innermost SMC fields K28 and K44. The BH map is based on the H I emission of the Galaxy. Table 3 lists the resulting $E(B-V)$ values. Except for K28, the cluster sample shows only small differences between the two colour excess estimates. The average of the BH values is 0.034 ± 0.023, while the typical reddening estimated by SFD for the SMC is 0.037. Given the large discrepancy for K28, we will derive metallicities based on both reddening values. For the other clusters, we use the BH values. We recall that an increase of the assumed reddening by $E(B-V) = 0.03$ decreases the derived metallicity by 0.12 dex (Bica et al. 1998).

Fig. 8 shows an example of a cluster CMD compared with the standard giant branches, while Table 3 lists the resulting [Fe/H] values. Note that the metallicity for L116 is very uncertain given the sparcity of giants and the uncertainty in its distance (we used a value of 18.2 based on its RGC mag.). As, for metallicities lower than [Fe/H] ≈ -0.5 dex, the red giant branches were derived using Galactic globular clusters with ages >10 Gyr, the calibration is not directly applicable to most of our SMC clusters because of the noticeable effect of the age differences on broad-band colours. Geisler & Sarajedini (1999) found that the age effect on metallicity derivation should be small or negligible for clusters $>\sim 5$ Gyr old. Bica et al. (1998) investigated the effect for younger clusters and found a mean offset of 0.4 dex, in the sense that the metallicities derived from the standard giant branch technique for younger clusters were too low compared with spectroscopically derived values. However, most members of their sample were only 1–2 Gyr old. Lacking further details, we correct our metallicities by +0.2 dex for clusters of 3–5 Gyr and +0.4 dex for clusters of 1–3 Gyr. It is important to note that the high reddening value for K28 takes into account the dust along the line of sight through the entire SMC body, and it would be appropriate for dereddening the cluster if it were behind the Small Cloud, which is probably not the case as judged from the position of its RGC. The iron-to-hydrogen ratio corresponding to SFD's colour excess appears in parentheses, and for further analysis we use the value based on the BH reddening. The metallicity uncertainties were estimated at $\sim$0.2 dex in all cases, including the uncertainty in deriving the original mean value, the uncertain age correction, and reddening and calibration errors.

4.2 Surrounding fields

Ages for surrounding fields were determined employing the same method described for clusters. As fields are in most cases obviously a composite of stellar populations with different ages, we measured the δT_1 values for the most populous turn-offs, as done for our LMC sample (Bica et al. 1998). To assess such turn-offs along MSs of the surrounding fields of K28 and K44, we applied the following criterion. First, in the Galactic foreground-cleaned CMD, we defined the region corresponding to the MS. This was accomplished by tracing a lower envelope composed of two straight lines and a reddest envelope shifting the lower envelope by +0.4 mag. The lines defining the lower envelope are given by the

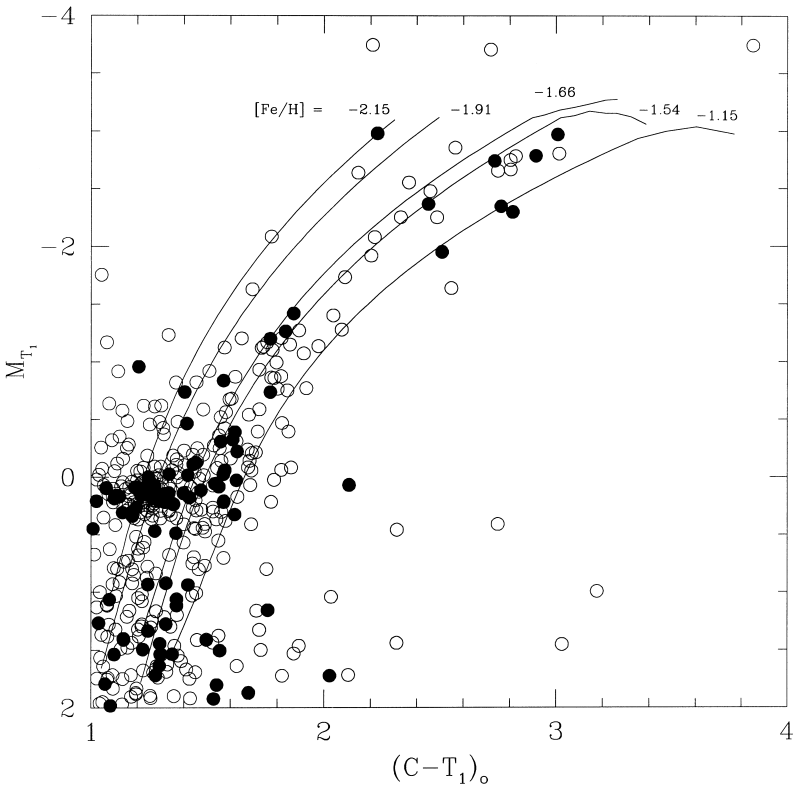

Figure 8. Metallicity derivation for the IAC K44. The cluster has been placed in the absolute T_1 magnitude–dereddened $(C-T_1)$ colour plane assuming an apparent distance modulus of 19.0 and a reddening of $E(B-V) = 0.03$. Standard giant branches from Geisler & Sarajedini (1999) are marked with their metallicity values.

expressions $T_1 = 18.0 \times (C - T_1 - \alpha_1) + 28.5$ and $T_1 = 4.4 \times (C - T_1 - \alpha_2) + 21.6$, where α_1 and α_2 are constants equal to 0.0 and 0.1 for K28 and L68, respectively. We then built MS luminosity functions by counting all the stars distributed in the previously delimited CMD zone and within intervals of $\Delta T_1 = 0.5$ mag. Assuming that the observed MS is the result of the superposition of different MSs, we considered the magnitude associated with each bin as that corresponding to a MS, the turn-off of which lies at that T_1 value. Such a MS is also assumed to have a uniform number of stars per magnitude interval. To obtain the number of stars per bin which only belong to the MS turn-off in that bin, we subtracted from each interval the number of stars counted in the following fainter bin. Negative values reflect either that the turn-off of the fainter bin is less populous than that of the adjacent brighter bin or incompleteness effects caused by reaching the limiting magnitude. The T_1 magnitude of the interval with the highest number of stars, after subtraction of fainter MS stars, was adopted as the turn-off magnitude of the most numerous stellar population of the surrounding cluster field. For the surrounding fields of L32 and L38, we directly measured δT_1 because their turn-offs are clearly visible in CMDs. The L116 surrounding field does not present any evidence of SMC features so that no age estimate was obtained. Table 2 lists the derived field ages. We point out that each field likely contains stars old enough that their turn-off is fainter than the limit of the data. The ages that we estimate for the fields correspond to the majority of detected stars. The more populated fields of K28 and K44 will certainly deserve detailed modelling to explore the age structure, but the basic age of the detected stars could be inferred.

Metallicities for the surrounding cluster fields were derived in the same manner as for clusters. We did not estimate the metallicity of the L116 field because of the lack of any SMC feature. To transform the observed (T_1, $C - T_1$) diagrams into the absolute [M_{T_1}, $(C - T_1)_o$] plane, we used the colour excesses $E(B - V)_{BH}$ listed in Table 3. The upper MSs of the clusters and their surrounding fields show a slight difference in colour, probably because of differences in the younger stellar population composition of these fields. The colour difference between the RGCs of the K28 and K44 fields is also less than 0.03 mag, which is in very good agreement with the cluster BH reddening difference. Fig. 9 shows a typical IAC field. Note that the fields generally showed a significant range in metallicity, amounting to ~0.4 dex (although some of this scatter can be explained by SMC asymptotic giant branch stars), and that the values quoted are crude means. The same metallicity correction required for age effects for IAC objects were applied as for the clusters. The final metal abundance values are listed in Table 3, where a colon denotes an uncertain value.

5 DISCUSSION

The five studied SMC clusters are spatially distributed along a curve that starts at the north-west of the SMC and crosses its bar almost perpendicular to the south-east. The SMC bar is approximately oriented in the south-west–north-east direction. L32, L38 and K28 are on the north-west side of the bar, while K44 and L116 are located on the other side (see Fig. 1). According to the derived ages, the cluster sample seems to be composed of objects distributed in two age groups with ages ~of 2.5 and 5.5 Gyr, respectively. Clusters in these age groups would also

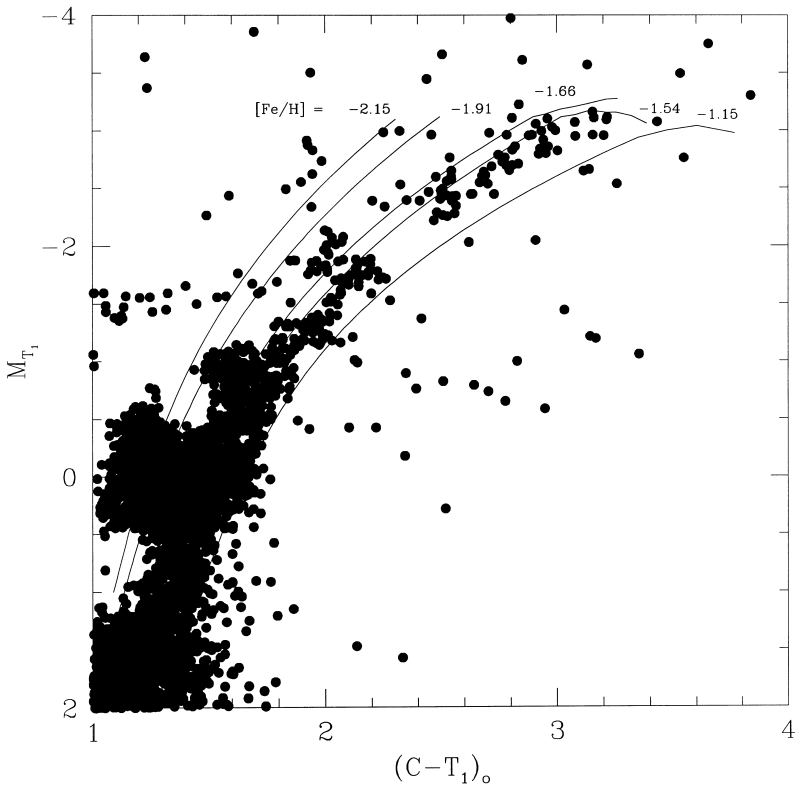

Figure 9. Metallicity derivation for the IAC field K44. The cluster field has been placed in the absolute T_1 magnitude–dereddened $(C - T_1)$ colour plane assuming an apparent distance modulus of 19.0 and a reddening of $E(B - V) = 0.03$. Standard giant branches from Geisler & Sarajedini (1999) are marked with their metallicity values.

appear spatially located in different SMC regions. The oldest clusters are preferably distributed on the north-west side of the bar, while the youngest ones are located on the other side. We checked this spatial age distribution by considering the ages of L113, K3, NGC 339, NGC 416, NGC 361, L1 and NGC 121 derived by MSF, because they are on the Zinn metallicity scale and used an age scale where L1 is 9 Gyr, i.e. the same age–metallicity scale adopted in the present study. Joining our five clusters with these additional seven clusters results in a sample of five and seven objects distributed on each side of the bar. Fig. 1 presents clusters from MSF with open triangles. The mean ages turned out to be (4.9 ± 1.7) Gyr ($n = 5$) and (6.8 ± 2.9) Gyr ($n = 7$) for the south-east and north-west groups, respectively. The derived mean ages are comparable within dispersions so that star formation processes and dynamical evolution have produced a homogeneous distribution. However the sample should be increased, and the present observations suggest that more IACs should turn up in future studies.

Cluster metallicities appear to follow an age–metallicity relation, because our most metal-rich objects are also the youngest clusters and the most metal-poor ones are the oldest ones of the sample. The mean metallicity of south-east and north-west cluster groups (MSF's clusters included) resulted in [Fe/H] = −1.28 ± 0.17 ($n = 5$) and −1.39 ± 0.21 ($n = 7$), respectively. If we did not include MSF's clusters, the mean metallicities would be [Fe/H] = −1.1 ± 0.10 ($n = 2$) and −1.35 ± 0.21 ($n = 3$) instead of −1.3 and −1.4, respectively. This result suggests that the oldest clusters in the south-east group are responsible for the most metal-poor averaged [Fe/H] value. In addition, this result also shows that there is no evidence of any bias, in the sense that clusters older than 5.0 Gyr should not have had their forming regions confined to some parts of the galaxy, but throughout the whole SMC body.

Our cluster sample considerably enlarges the number of SMC IACs and old clusters with ages and metallicities on the same system, thus providing us with a sufficient large number of objects with which to investigate their age distribution. Fig. 10 shows the resulting histogram for 11 SMC clusters (seven clusters from MSF and four clusters from this study). As can be seen, it would appear

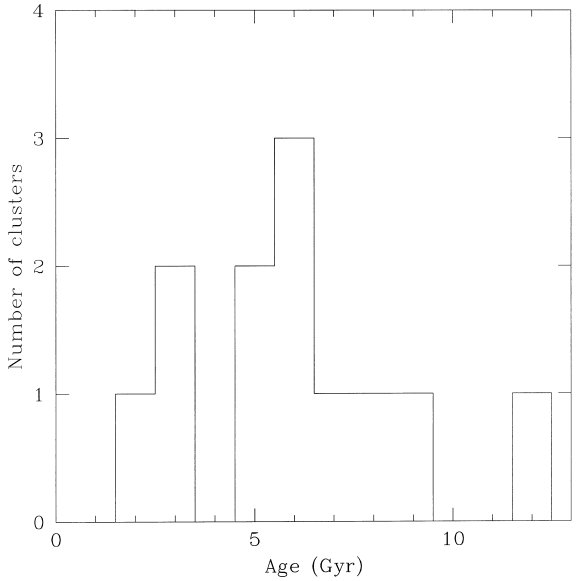

Figure 10. The age distribution of SMC clusters older than 1 Gyr derived from MFS and the present cluster sample.

that clusters have been formed during the entire SMC lifetime, with some epochs with more intense cluster formation activity. In particular, Fig. 10 reveals that there could be at least two important cluster formation epochs at ∼3 and ∼6 Gyr qualitatively in line with the findings of Rich et al. (2000). The resulting absolute distance modulus for L116 is $(m - M)_o = 17.8$ implying a distance from the Sun $d_\odot = 36$ kpc. The cluster appears to be in the foreground of the SMC, and possibly also slightly closer than the LMC, assuming that the latter is at 50 kpc (see Bica et al. 1998). The projected distance from the LMC bar is ≈16°, which at the LMC distance is ≈14 kpc. This value is smaller than the derived cluster distance to the SMC ≈20 kpc assuming the SMC distance to the Sun as 63 kpc. This suggests that the cluster belongs instead to the LMC, although deeper observational data are really required to sort out the nature of this object. Two Population II globular clusters considered as LMC members are as distant: Reticulum at 15.°7 and NGC 1841 at 20.°3 convert at the LMC distance to 14.0 and 18.5 kpc from the LMC bar respectively. The outermost LMC IAC cluster known is OHSC 37 (Bica et al. 1998) at a projected distance from the LMC bar centre of ≈13°, or 11.5 kpc. Population II globular clusters are expected at large distances because they may be part of an extended spheroid, but such far-away intermediate-age clusters may instead be explained by (i) cluster scattering during LMC–SMC interactions or (ii) star cluster formation during early LMC–SMC interactions in features such as bridges and tidal arms.

A comparison between the derived cluster and surrounding field ages shows that clusters are projected towards SMC fields generally composed of a similar stellar population; the difference between them being $\Delta t_{(\mathrm{cluster-field})} = -0.5 \pm 1.0$ Gyr. The fields of K28 and K44, besides the intermediate-age component denoted by the clump and RGB, present a young component as revealed by the blue MS extending well above the clump level. This shows that the edge of the SMC main body has been active in star formation until quite recently. The projected linear distances from the bar centre for L32 and L38 are 4.6 and 3.6 kpc, respectively, and at such distances the SMC field population is clearly present (Fig. 6). However, the CMDs of these more distant fields do not show young components; at such distances the intermediate ages prevail. The field around L116 does not show evidence of an SMC population, the field appearing as foreground Galactic stars. We recall that at the SMC distance the linear separation would be 6.7 kpc. Similarly, metallicities of both clusters and their surrounding fields seem to be indistinguishable within the errors, with a difference of $\Delta[\mathrm{Fe/H}]_{(\mathrm{cluster-field})} = 0.04 \pm 0.17$ dex.

Finally, we studied the chemical enrichment of the SMC using ages and metallicities of the seven star clusters observed by MSF and our present IAC sample. We included five young SMC clusters from Da Costa & Hatzidimitriou (1998), which represent the present-day properties of the SMC, because they were also included by MSF in their fig. 13. Fig. 11 shows the resulting age–metallicity relationship, where we present previously studied clusters and those discussed in this paper with open and filled circles, respectively. The error bars are also included. Only one cluster in our sample (L38) is as metal-poor as those of MSF. Six of eight clusters older than 5.0 Gyr have metallicities in the range $-1.7 \leq [\mathrm{Fe/H}] \leq -1.4$, which could suggest that the chemical enrichment would not have been very efficient until the last 5 Gyr. After that period, the age–metallicity relation would seem to undergo a change in its mean metallicity, as the metal content increases in average from [Fe/H] ∼ −1.5 up to −1.1 dex. We compare our age–metallicity relation with two theoretical models

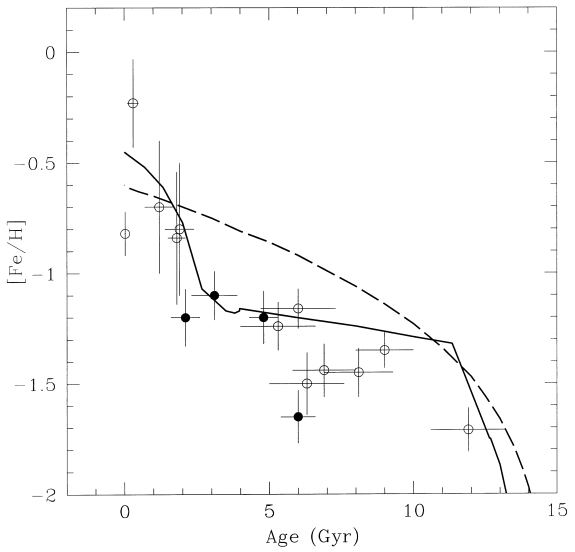

Figure 11. Age–metallicity relationship for star clusters in the SMC. Open circles represent data previously published by Da Costa & Hatzidimitriou (1998) and Mighell et al. (1998), while filled circles correspond to the SMC clusters studied in this paper. Error bars are also included. The data are compared with the closed box continuous star formation model (dashed line) computed by Da Costa & Hatzidimitriou (1998) for an assumed present-day metallicity of −0.6 for the SMC, and the bursting model (solid line) of Pagel & Tautvaišienė (1998).

of the SMC star formation history. The dashed line represents a simple closed system with continuous star formation under the assumption of chemical homogeneity (Da Costa & Hatzidimitriou 1998), whereas the solid line depicts the bursting star formation history of Pagel & Tautvaišienė (1998). The appearance of Fig. 11 indicates that a closed-box continuous star formation model is a poor representation of the SMC star formation history. Instead, the refinement of the Pagel & Tautvaišienė bursting model is closer to the observed cluster data points. In particular, MSF suggest that the bursting model would be a better fit if the initial star formation epoch lasted 2 Gyr instead of 2.7 Gyr as originally assumed by the Pagel & Tautvaišienė models. Our additional cluster data points corroborate this modification by MSF. Furthermore, we note that Da Costa (1999) has emphasized one specific weakness of the Pagel & Tautvaišienė (P&T) model. He points out that between ∼4 and ∼12 Gyr, the P&T model predicts a star formation rate that is likely to be too low to produce the relatively large number of star clusters present in this age range. However, Da Costa (1999) also notes that this apparent difficulty can be resolved if the star formation rate in the model is increased to a level that is adequate to produce the numbers of star clusters and, at the same time, the abundance of the ISM is diluted by the infall of primordial or low-abundance gas, which would serve to keep the overall metal abundance nearly constant during this time interval. Given the past interactions of the SMC with the LMC and the Milky Way, the possibility that the SMC was not a perfect closed box is quite plausible.

6 CONCLUSIONS

New Washington photometry was presented for five clusters (L32, L38, K28, K44 and L116) and surrounding fields projected on to the SMC body and outskirts. On the basis of their colour–magnitude diagrams we have determined age and metallicity for both clusters and respective surrounding fields. All clusters turned out to be of intermediate age. One of them (L116) probably does not belong to the SMC, as indicated by its proximity to the LMC. Including clusters and fields, the range of ages found was 2.1 to 6.7 Gyr and that of metallicities was $-1.70 < [Fe/H] < -0.90$. The whole sample of known intermediate-age and old SMC clusters with ages and metallicities determined on a uniform scale has now increased to 11.

The frequency distribution of clusters with age suggests two cluster formation epochs: one at 3 and another at 6 Gyr, although more cluster observations are needed for a better definition of these events. On the basis of the RGC magnitude, a distance of 36 kpc to L116 was obtained. Assuming 8.5 kpc for the Sun–Galactic centre distance, the distance of the cluster from the Galactic centre is ≈34 kpc. The derived deprojected distance of L116 to the LMC is 18 kpc and to the SMC is 27 kpc. Therefore, the cluster is in the Galactic halo and closer to the LMC than to the SMC. There are 10 Galactic globular clusters farther than ≈34 kpc from the Galactic centre. However, old Galactic open clusters, more similar to L116, are not found that far away. In the LMC, the farthest known intermediate-age cluster is OHSC 37, at more than 10 kpc from the LMC bar centre. This suggests that the properties of the intermediate-age cluster L116, including its distance, are more compatible with LMC membership.

Concerning the SMC field population, it is clear that a young stellar population component is mixed with the intermediate-age one in the inner fields at projected distances of 1.2 kpc from the SMC centre (K28 and K44 fields). In the outer fields associated with L32 and L38 (at 5 kpc and 4 kpc respectively), the intermediate-age component is dominant and the young component does not show up. This demonstrates that recent star formation has occurred in regions closer to the SMC body.

ACKNOWLEDGMENTS

The authors thank the CTIO staff for their kind hospitality during the observing run. They also acknowledge Carlos Dutra, who provided the reddening values for the cluster sample from the SFD dust map, and thank the referee for valuable comments and suggestions. AEP and JJC acknowledge the Argentinian institutions CONICET and Agencia Nacional de Promoción Científica y Tecnológica (ANPCyT) for their partial support. EB also acknowledges the Brazilian institution CNPq for its support. DG acknowledges financial support for this project received from CONICYT through Fondecyt grants 1000319 and 8000002, and from the Universidad de Concepción through research grant No. 99.011.025.

REFERENCES

Bertelli G., Bressan A., Chiosi C., Fagotto F., Nasi E., 1994, A&AS, 106, 275
Bica E., Schmitt H. R., 1995, ApJS, 101, 41
Bica E., Geisler D., Dottori H., Clariá J. J., Piatti A. E., Santos J. F. C., Jr, 1998, AJ, 116, 723
Burstein D., Heiles C., 1982, AJ, 87, 1165
Canterna R., 1976, AJ, 81, 228
Cioni M. R., van der Marel R. P., Loup C., Habing H. J., 2000, A&A, 359, 601
Da Costa G. S., 1991, in Haynes R., Milne D., eds, IAU Symp. 148, The Magellanic Clouds. Kluwer, Dordrecht, p. 183
Da Costa G. S., 1999, in Chu Y. H., Hesser J. E., Suntzeff N., eds, IAU

Symp. 190, New Views of the Magellanic Clouds. Astron. Soc. Pac., San Francisco, p. 397
Da Costa G. S., Armandroff T. E., 1990, AJ, 100, 162
Da Costa G. S., Hatzidimitriou D., 1998, AJ, 115, 1934
Dutra C. M., Bica E., Clariá J. J., Piatti A. E., 1999, MNRAS, 305, 373
Elson R. A. W., Fall S. M., 1985, ApJ, 299, 211
Feast M. W., 1995, in van der Kruit P. C., Gilmore G., eds, IAU Symp. 164, Stellar Populations. Kluwer, Dordrecht, p. 153
Gallart C., 1998, ApJ, 495, L43
Geisler D., 1996, AJ, 111, 480
Geisler D., Sarajedini A., 1999, AJ, 117, 308
Geisler D., Bica E., Dottori H., Clariá J. J., Piatti A. E., Santos J. F. C., Jr, 1997, AJ, 114, 1920
Hodge P. W., 1960, ApJ, 131, 351
Hodge P. W., 1961, ApJ, 133, 413
Ibata R. A., Lewis G. F., Beaulieu J.-P., 1998, ApJ, 509, L29
Jensen J., Mould J., Reid N., 1988, ApJS, 67, 77
Kron G. E., 1956, PASP, 68, 125
Lauberts A., 1982, The ESO/Uppsala Survey of the ESO (B) Atlas. European Southern Observatory Garching bei Munchen
Lindsay E. M., 1958, MNRAS, 118, 172
Mateo M., Hodge P. W., Schommer R. A., 1986, ApJ, 311, 113
Mighell K. J., Sarajedini A., French R. S., 1998, AJ, 116, 2414 (MSF)
Mould J., Da Costa G. S., Crawford M. D., 1984, ApJ, 280, 595
Olsen K. A., Hodge P. W., Mateo M., Olszewski E. W., Schommer R. A., Suntzeff N. B., Walker A. R., 1998, MNRAS, 300, 665
Olszewski E. W., Schommer R. A., Aaronson M., 1987, AJ, 93, 565
Olszewski E. W., Schommer R. A., Suntzeff N. B., Harris H. C., 1991, AJ, 101, 515
Olszewski E. W., Suntzeff N. B., Mateo M., 1996, ARA&A, 34, 511
Pagel B. E. J., Tautvaišienė G., 1998, MNRAS, 299, 535
Phelps R. L., Janes K. A., Montgomery K. A., 1994, AJ, 107, 1079
Piatti A. E., Geisler D., Bica E., Clariá J. J., Santos J. F. C., Jr, Sarajedini A., Dottori H. A., 1999, AJ, 118, 2865
Rich R. M., Da Costa G. S., Mould J., 1984, ApJ, 286, 517
Rich R. M., Shara M., Fall S. M., Zurek D., 2000, AJ, 119, 197 (RSFZ)
Sarajedini A., 1998, ApJ, 116, 738
Schlegel D. J., Finkbeiner D. P., Davis M., 1998, ApJ, 500, 525
Stetson P. B., 1994, PASP, 106, 250
Stryker L. L., Da Costa G. S., Mould J. R., 1985, ApJ, 29, 545
Suntzeff N. B., Schommer R. A., Olszewsky E. W., Walker A. R., 1992, AJ, 104, 1743
van den Bergh S., 1991, ApJ, 369, 1
Walker A. R., 1998, AJ, 116, 220
Westerlund B. E., 1997, The Magellanic Clouds. Cambridge Univ. Press, Cambridge
Zaritsky D., Lin D. N. C., 1997, AJ, 114, 2545
Zinn R., 1985, ApJ, 293, 424

This paper has been typeset from a TEX/LATEX file prepared by the author.